Supporting Information

Surface Hydroxylation Induced by Alkaline-earth Metal Doping in NiO Nanocrystals and Its Application in Achieving a Wide Temperature Operation Window of Preferential CO Oxidation

Huixia Li,[a] Liping Li,[a]　Shaofan Fang,[b]　Jianghao Wang,[b] Shaoqing Chen,[c]　Xinsong Huang,[b]　Zhihua Leng,[a] Guangshe Li*,[a]

[a]State Key Laboratory of Inorganic Synthesis and Preparative Chemistry, College of Chemistry, Jilin University, Changchun 130012, P.R. China.

[b]Key Laboratory of Design and Assembly of Functional Nanostructures, Fujian Institute of Research on the Structure of Matter, Fuzhou 350002, P. R. China.

[c]Department of Materials Science and Engineering, Southern University of Science and Technology, Shenzhen, Guangdong 518055, China

Table of contents

Figure S1. TEM images of $Ni_{0.5}Mg_{0.5}O$ solid solution via the precipitate process of Mg after Ni.

As shown in Figure S1, we carried out the precipitate process of Mg after Ni to obtain the $Ni_{0.5}Mg_{0.5}O$ samples. Although the sample presented the irregular nanosheets morphology, the nanosheets were severely accumulational which could severely hinder the exposure of active site and the support of noble metals.
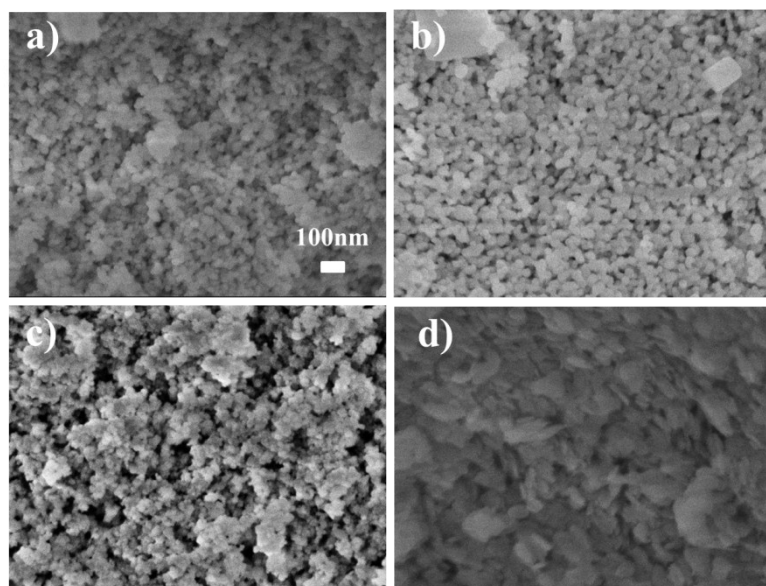
Figure S2. Scanning electron micrographs of (a) the $Ni_{0.5}Mg_{0.5}O$ support, (b) $Pt/Ni_{0.5}Mg_{0.5}O$ catalyst (c) Pt/NiO and (d) $Pt/Mg(OH)_2$ catalyst.

SEM images of the catalysts are shown in Figure S1. $Ni_{0.5}Mg_{0.5}O$ and $Pt/Ni_{0.5}Mg_{0.5}O$ catalysts (Figures S1a and S1b) present uniform size. Although Pt/NiO catalyst (Figure. S1c) exhibited a similar morphology to $Pt/Ni_{0.5}Mg_{0.5}O$ catalyst, the nanosheets in Pt/NiO exhibited a slight agglomeration. $Pt/Mg(OH)_2$ catalyst consisted of hexagonal nanoflakes (Figure S1d). The average size of hexagonal nanoflakes was larger than those of other catalysts.
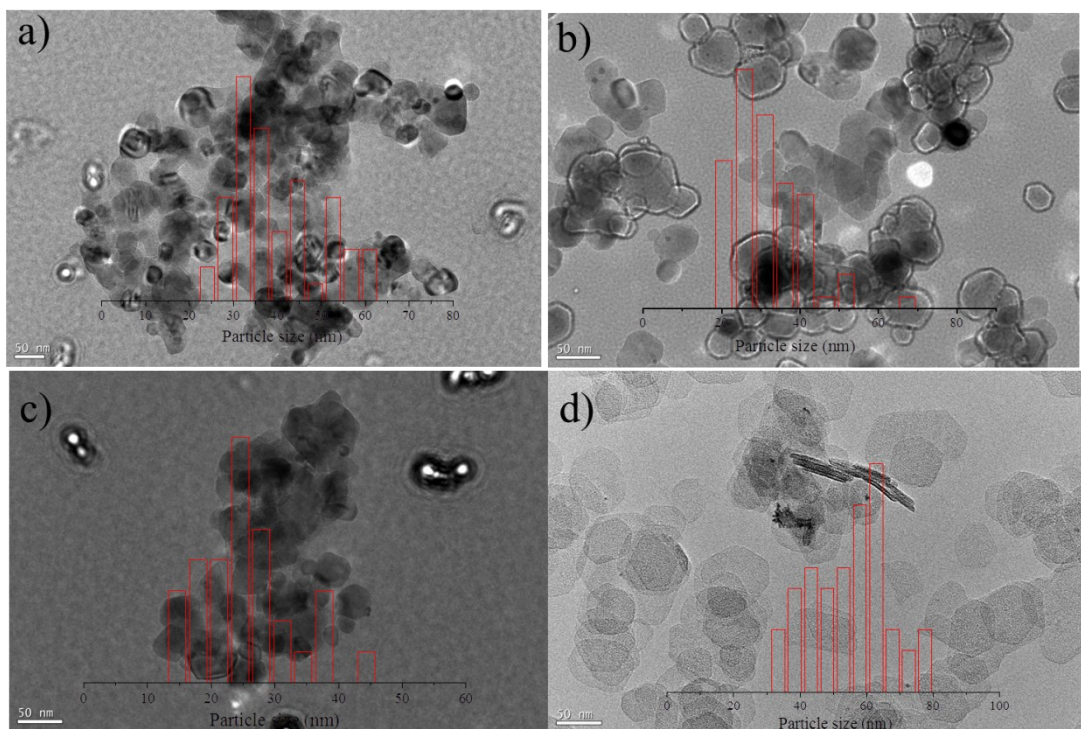
Figure S3. TEM images of (a) $Ni_{0.5}Mg_{0.5}O$, (b) $Pt/Ni_{0.5}Mg_{0.5}O$, (c) Pt/NiO, and (d) $Pt/Mg(OH)_2$ that show the estimated particle sizes.

The particle size distribution for $Ni_{0.5}Mg_{0.5}O$ support is about 30-40 nm. After supporting Pt, particle size distribution has not changed. This result indicates that supporting Pt catalyst had no distinct effect on the particle size. The particle size distributions for Pt/NiO and $Pt/Mg(OH)_2$ catalysts, are about 20-30 and 50- 60 nm, respectively. The particle size distribution of $Pt/Ni_{0.5}Mg_{0.5}O$ catalyst is between Pt/NiO and $Pt/Mg(OH)_2$.
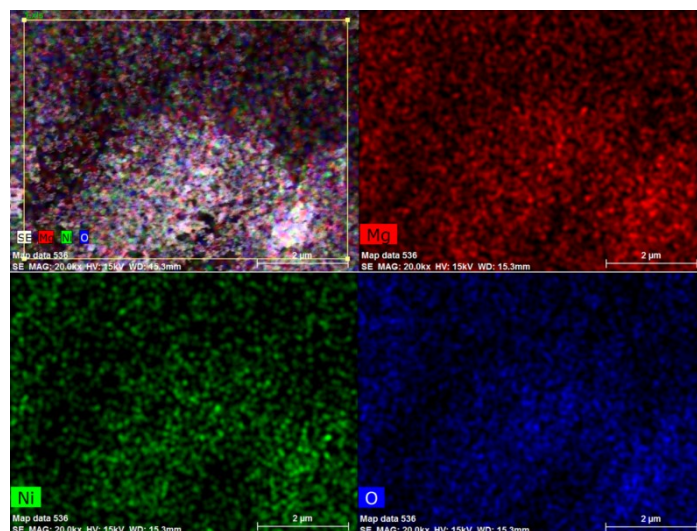
Figure S4. SEM elemental mapping of $Ni_{0.5}Mg_{0.5}O$ solid solution.
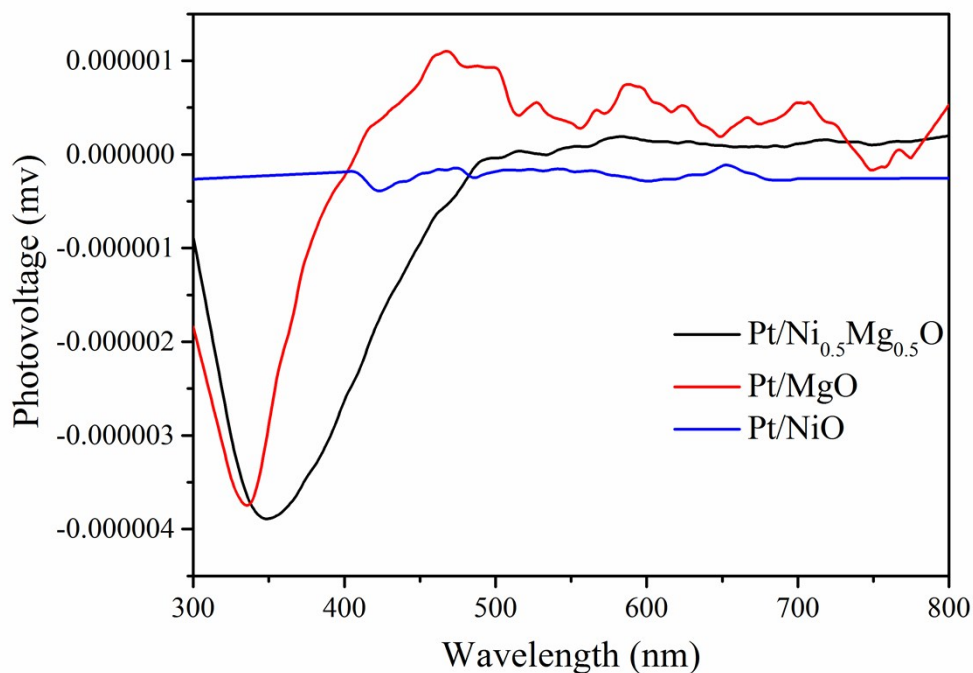
Figure S5. Surface photovoltage spectra (SPV) of Pt/Ni$_{0.5}$Mg$_{0.5}$O, Pt/MgO and

Pt/NiO catalysts.

For the SPV response, a positive signal implies a positive charge accumulation at the

surface of the sample. On the contrary, a negative signal is produced due to the

negative charge accumulation at the surface. For Pt/Ni$_{0.5}$Mg$_{0.5}$O catalyst, a weak

negative SPV response arises between 300 and 488 nm, which implies a negative

charge accumulation at the surface. Pt/MgO performs the similar behavior to

Pt/Ni$_{0.5}$Mg$_{0.5}$O. However, Pt/NiO has no SPV response. Therefore, the electron is

supplied from the magnesium ions to the active metal in the catalyst and strengthens

CO adsorption.
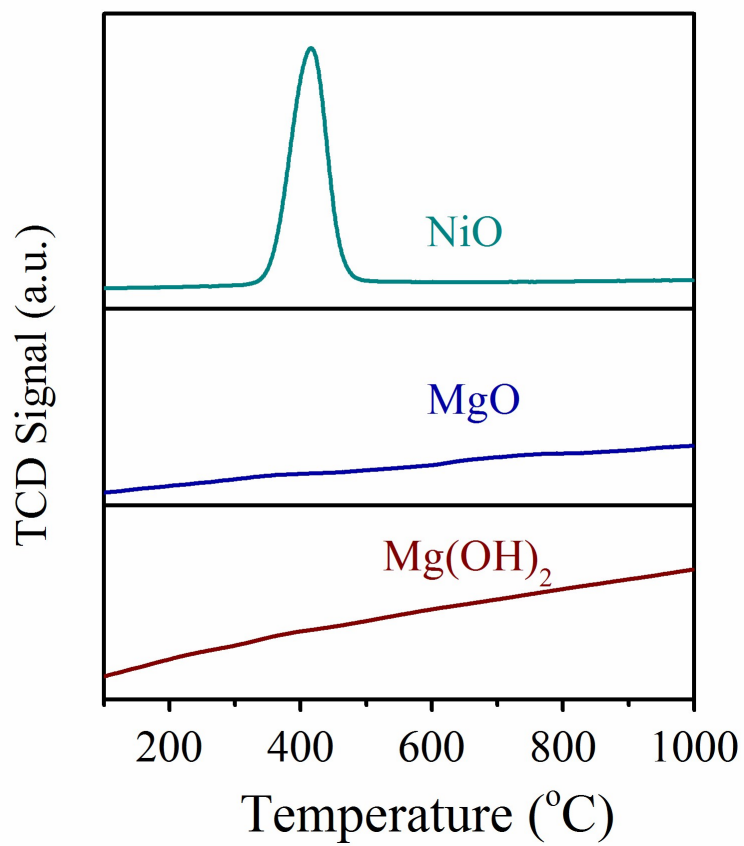
Figure S6. H_2-TPR profiles of the contrast samples NiO, MgO, and $Mg(OH)_2$.
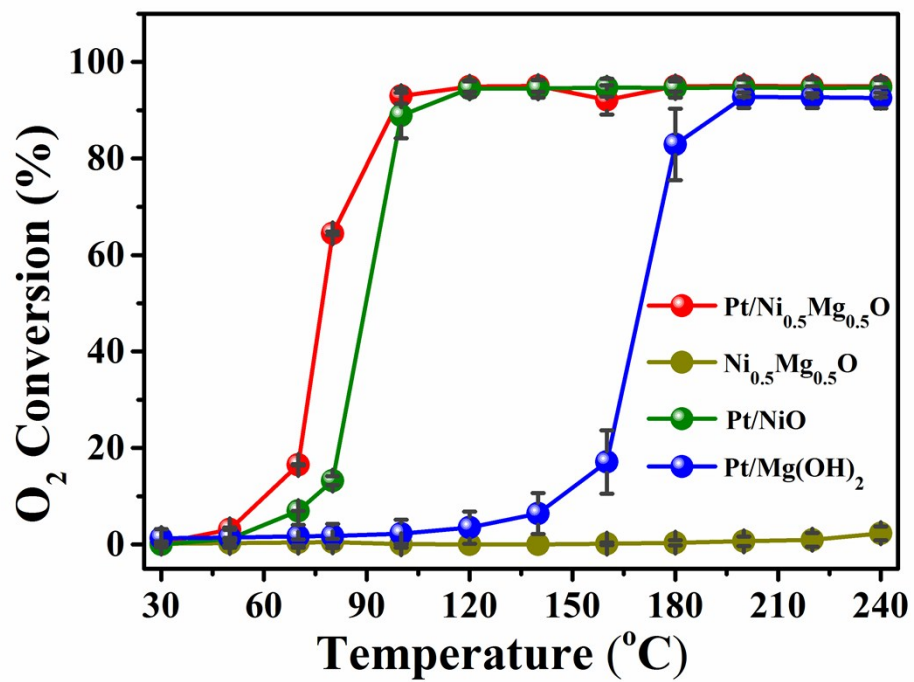
Figure S7. O_2 conversion of all catalysts.
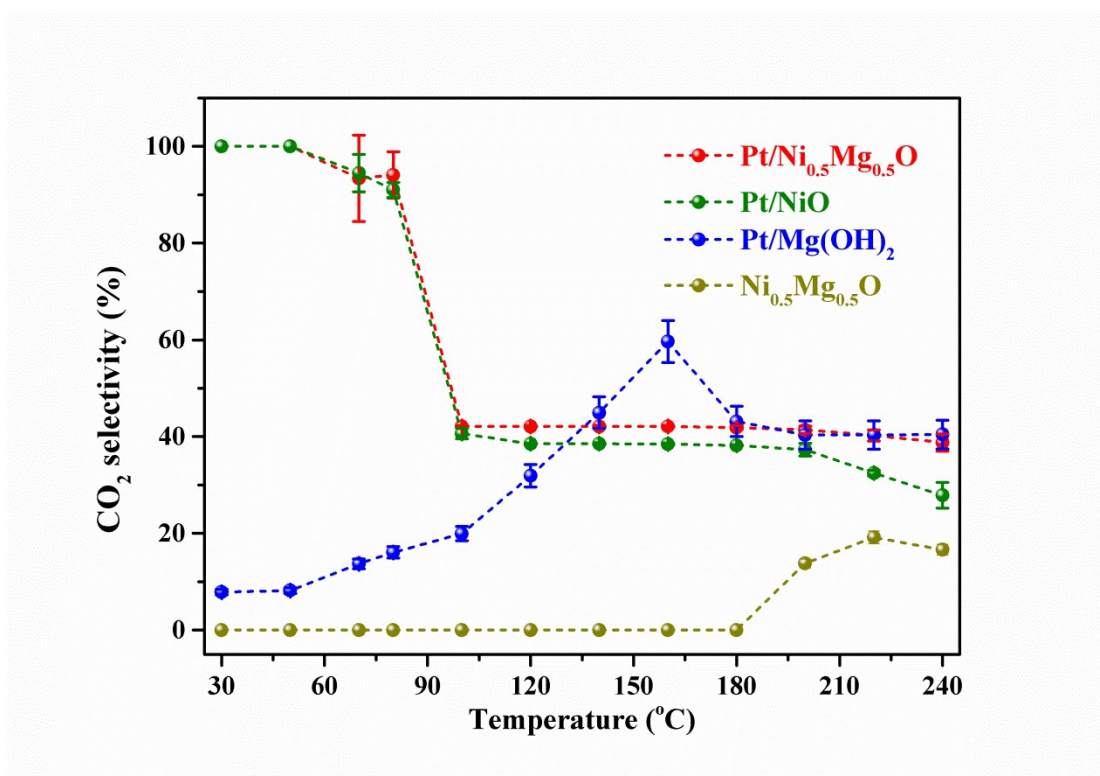
Figure S8. CO_2 selectivity of four catalysts. PROX reactions were performed over the

four catalysts at $C:O_2$ ratios of 1:1.25 and a GHSV of 80000 h^{-1}.
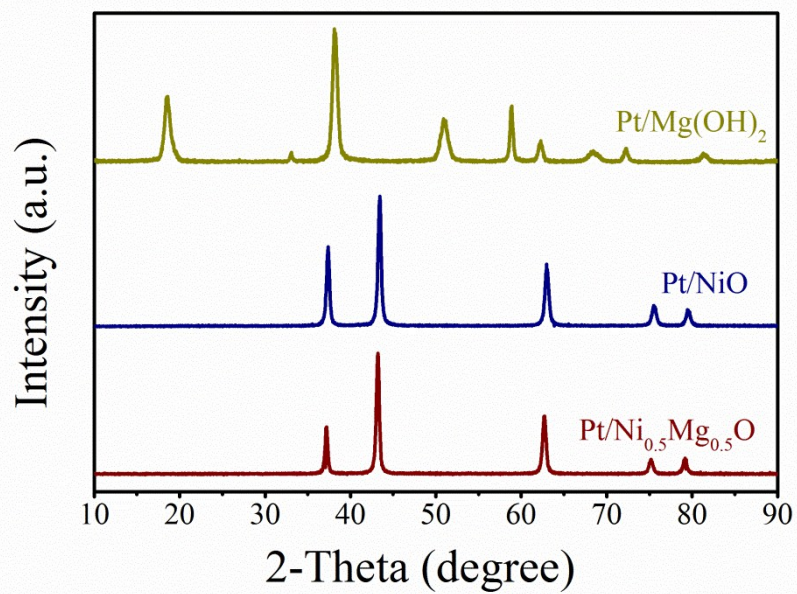
Figure S9. XRD patterns of the catalysts used Pt/Ni$_{0.5}$Mg$_{0.5}$O, Pt/NiO, and

Pt/Mg(OH)$_2$.
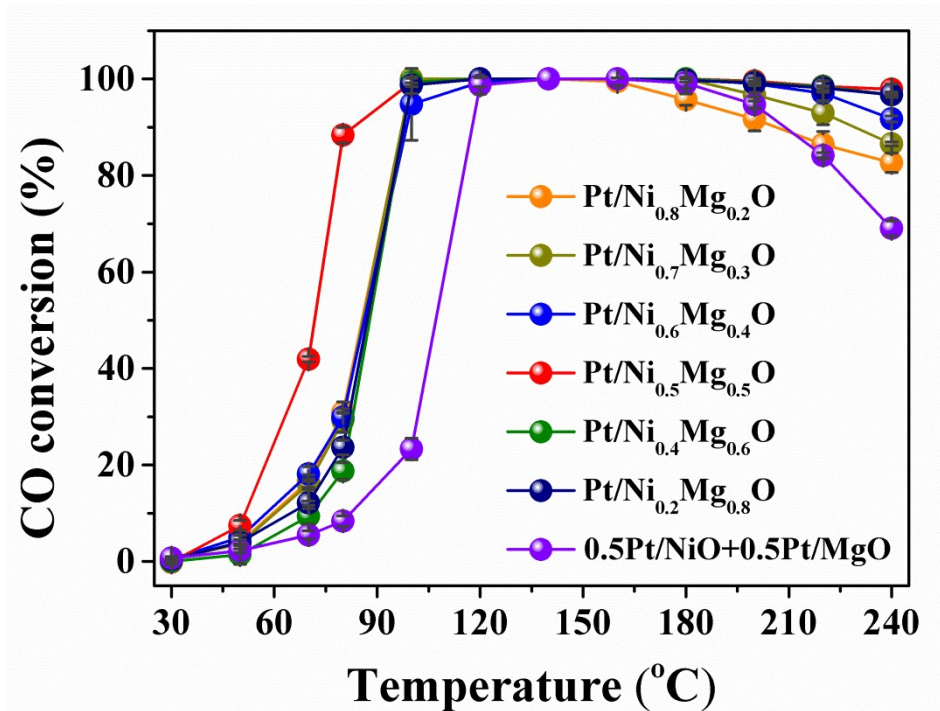
Figure S10. CO conversions of Pt supported $Ni_{1-x}Mg_xO$ (0, 0.2, 0.3, 0.4, 0.5, 0.6, 0.8)

solid solutions for CO oxidation reactions in H_2-rich condition.
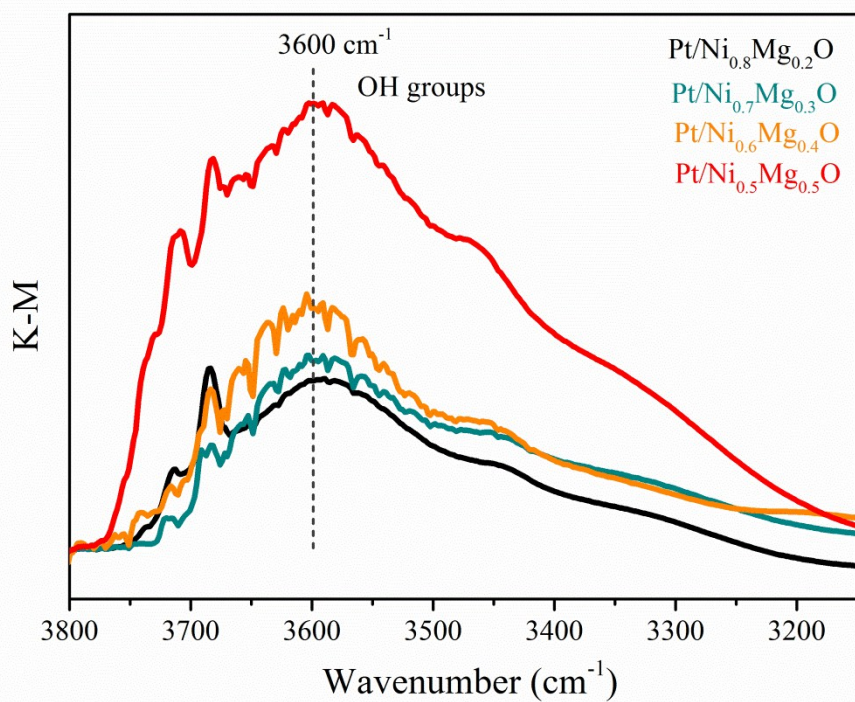
Figure S11. DRIFTS recorded for Pt/Ni$_{1-x}$Mg$_x$O (x = 0.2, 0.3, 0.4, 0.5) under the CO-PROX measurement conditions (i.e., 1 % CO, 1.25 % O$_2$ and 50 % H$_2$ in He balance) at 30 °C.
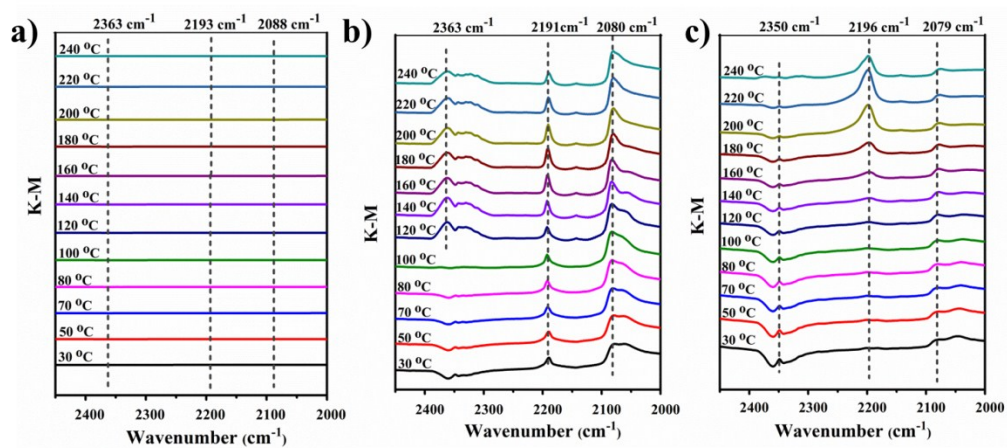
Figure S12. DRIFT spectra recorded for (a) $Ni_{0.5}Mg_{0.5}O$, (b) Pt/NiO, and (c) $Pt/Mg(OH)_2$ as a function of temperature under operando PROX conditions (i.e., 1 % CO, 1.25 % O_2 and 50 % H_2 in He balance).
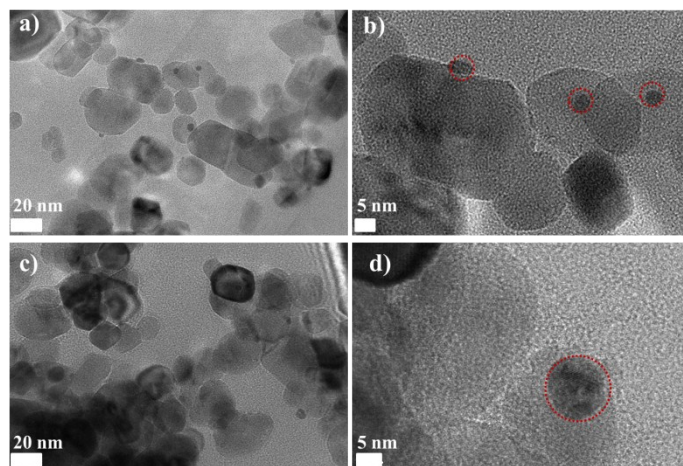
Figure S13. TEM images of the Pt/Ni$_{0.5}$Mg$_{0.5}$O and Pt/NiO after the stability test for 50 h.
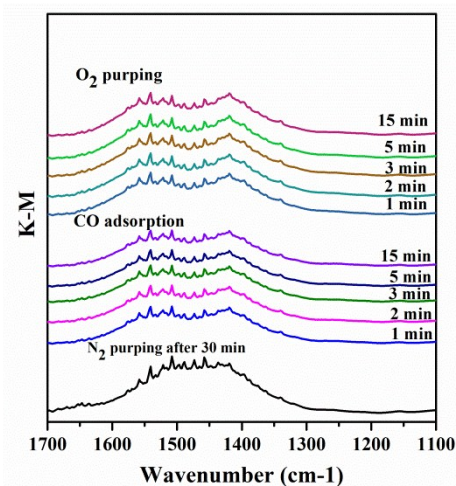
Figure S14. In situ DRIFTS study of N_2 purging, CO adsorption, O_2 removal on the Pt/Ni$_{0.5}$Mg$_{0.5}$O catalyst. (CO flow rate, 10 mL min^{-1}; catalyst mass, 20 mg; temperature, 140 ^{o}C).

In situ DRIFTS was carried out to identify the active species by analyzing the spectral range of 1700-1100 cm^{-1}. In a typical steady test, the powder sample (ca. 20 mg) was purged in N_2 for 30 min at room temperature and a background spectrum was collected via 48 scans at 4 cm^{-1} resolution. The reaction gas with 10 % CO/N_2 was introduced into the in situ chamber (10 mL min^{-1}) and heated to 140 ^{o}C. Once the CO adsorption lasted 15 min, the gas channel was switched immediately to 20 % O_2/N_2. These peaks hardly were observed change significantly when undergo the process of 10 % CO/N_2 shifting to 20 % O_2/N_2 compared to the treatment of N_2. The reason for this phenomenon is the presence of surface bicarbonates, which have lower thermal stability in comparison to carbonate species. The surface bicarbonates would favor a faster desorption of CO_2, leaving the surface available for further chemisorptions, through which the CO oxidation is accelerated.

Table S1. Particulate properties of the catalysts used.

Samples	Surface area (m²/g)	Pore volume (cm³/g)	Pore diameter (nm)
$Pt/Ni_{0.5}Mg_{0.5}O$	24	0.14	27
$Ni_{0.5}Mg_{0.5}O$	27	0.13	26
Pt/NiO	19	0.11	22
$Pt/Mg(OH)_2$	73	0.43	19

Table S2. Structural Refinement Results for Pt/$Ni_{1-x}Mg_xO$ Using GSAS softwave

Samples	Cell parameters	Rp	Rwp	X^2
	a (Å)			
Pt/NiO	4.1795(8)	0.0618	0.0839	4.418
Pt/$Ni_{0.8}Mg_{0.2}O$	4.1839(8)	0.0438	0.0588	2.845
Pt/$Ni_{0.7}Mg_{0.3}O$	4.1872(1)	0.0507	0.0668	3.703
Pt/$Ni_{0.6}Mg_{0.4}O$	4.1910(2)	0.0594	0.0851	4.778
Pt/$Ni_{0.5}Mg_{0.5}O$	4.1915(7)	0.0490	0.0694	3.429
Pt/$Ni_{0.4}Mg_{0.6}O$	4.1945(6)	0.0385	0.0542	3.814
Pt/$Ni_{0.2}Mg_{0.8}O$	4.1995(6)	0.0517	0.0749	4.532
Pt/ MgO	4.2087(6)	0.0485	0.0697	2.250

Table S3. Comparison of catalytic performance in CO-PROX over $Pt/Ni_{0.5}Mg_{0.5}O$ and those catalysts reported in literature.

Sample	Pt loading wt. %	Amount of catalyst (mg)	Space Velocity $(ml.g_{cat}^{-1}.h^{-1})$	Operation temperature window (CO conversion >99.0%)	ref
$Pt/Ni_{0.5}Mg_{0.5}O$	0.5	50	80000	100-220 °C	This work
Pt/NiO	0.5	50	80000	100-180 °C	This work
$Pt/Mg(OH)_2$	0.5	50	80000	200-240 °C	This work
$Pt/Ti_{0.5}Ce_{0.5}O_2$	0.6	100	17000	-	[1]
Pt-Ni-Al	0.5	undefined	12,000	200 °C	[2]
Pt/Co_3O_{4-x}	2.0	undefined	42857	110–130 °C	[3]
Pt-Ni/CNT-OX	2.0	50	48,000	95–120 °C	[4]
$Pt-Mg/Al_2O_3$	2.0	undefined	60000	-	[5]
$M–Pt–Ni/Al_2O_3$	1.0	undefined	16000	100-150 °C	[6]
$Pt/xCeO_2–(1−x)Nb_2O_5$	1.0	100	17000	-	[7]
Pt_3Co/MgO	3.0	50	-	120-160 °C	[8]
PtFeNi/CNTs-p	3.0	60	25000	-	[9]
$Pt/CuCrO_x$	2.0	100	60000	160-200 °C	[10]
$Pt–Ni/GMMSiO_2$	2.0	100	24000	95-120 °C	[11]

Reference

1. Rico-Francés, S.; Sepúlveda-Escribano, A.; Ramos-Fernandez, E. V., Ti x Ce (1-x) O 2 as Pt support for the PROX reaction: Effect of the solvothermal synthesis., *Int. J. Hydrogen Energ.,* 2017, 42 (49), 29262-29273.

2. Mohamed, Z.; Dasireddy, V. D. B. C.; Singh, S.; Friedrich, H. B., The preferential oxidation of CO in hydrogen rich streams over platinum doped nickel oxide catalysts. *Appl. Catal. B: Environ.,* 2016, **180**, 687-697.

3. Nguyen, L.; Zhang, S.; Yoon, S. J.; Tao, F. F., Preferential Oxidation of CO in H2on Pure Co_3O_{4-x} and Pt/Co_3O_{4-x}. *ChemCatChem,* 2015, **7** (15), 2346-2353.

4. Lu, S.; Zhang, C.; Liu, Y., Carbon nanotube supported Pt–Ni catalysts for preferential oxidation of CO in hydrogen-rich gases, *Int. J. Hydrogen Energ.,* 2011, **36** (3), 1939-1948.

5. Cho, S.-H.; Park, J.-S.; Choi, S.-H.; Kim, S.-H., Effect of magnesium on preferential oxidation of carbon monoxide on platinum catalyst in hydrogen-rich stream, *J.Power Sources,* 2006, **156** (2), 260-266.

6. Lu, S.; Liu, Y.; Wang, Y., Meso-macro-porous monolithic Pt-Ni/Al_2O_3 catalysts used for miniaturizing preferential carbon monoxide oxidation reactor, *Chem. Commun,* 2010, **46** (4), 634-6.

7. Jardim, E. O.; Rico-Francés, S.; Coloma, F.; Anderson, J. A.; Ramos-Fernandez, E. V.; Silvestre-Albero, J.; Sepúlveda-Escribano, A., Preferential oxidation of CO in excess of H_2 on Pt/CeO_2–Nb_2O_5 catalysts, *Appl. Catal. A- Gen.,* 2015, **492**, 201-211.

8. Furukawa, S.; Ehara, K.; Komatsu, T., Unique reaction mechanism of preferential oxidation of CO over intermetallic Pt_3Co catalysts: surface-OH-mediated formation of a bicarbonate intermediate, *Catal. Sci. Technol,* 2016, **6** (6), 1642-1650.

9. Chen, L.; Bao, Y.; Sun, Y.; Ma, D.; Ye, D.; Huang, B., The graphitic carbon strengthened synergetic effect between Pt and FeNi in CO preferential oxidation in excess hydrogen at low temperature, *Catal. Sci. Technol,* 2016, **6** (1), 98-106.

10. Deng, Y.; Wang, T.; Zhu, L.; Jia, A.-P.; Lu, J.-Q.; Luo, M.-F., Enhanced performance of CO oxidation over Pt/$CuCrO_x$ catalyst in the presence of CO 2 and H 2 O, *Appl. Surf. Sci.,* 2018, **442**, 613-621.

11. Niu, T.; Zhao, W. W.; Liu, G. L.; Cao, A.; Zhang, L. H.; Liu, Y., The graphene-meso-macroporous SiO_2 supported Pt–Ni alloy nanocatalyst for preferential oxidation of CO in H_2-rich gases, *Int. J. Hydrogen Energ.,* 2014, **39** (33), 18929-18939.